

This is the accepted manuscript made available via CHORUS. The article has been published as:

Coherence and Raman Sideband Cooling of a Single Atom in an Optical Tweezer

J. D. Thompson, T. G. Tiecke, A. S. Zibrov, V. Vuletić, and M. D. Lukin

Phys. Rev. Lett. **110**, 133001 — Published 26 March 2013

DOI: [10.1103/PhysRevLett.110.133001](https://doi.org/10.1103/PhysRevLett.110.133001)

Coherence and Raman sideband cooling of a single atom in an optical tweezer [v6.2]

J.D. Thompson*,¹ T.G. Tiecke*,^{1,2} A.S. Zibrov,¹ V. Vuletić,² and M.D. Lukin¹

¹*Department of Physics, Harvard University, Cambridge, MA 02138*

²*Department of Physics, MIT-Harvard Center for Ultracold Atoms, and Research Laboratory of Electronics, Massachusetts Institute of Technology, Cambridge, Massachusetts 02139*

(Dated: February 13, 2013)

We investigate quantum control of a single atom in a tightly focussed optical tweezer trap. We show that inevitable spatially varying polarization gives rise to significant internal-state decoherence, but that this effect can be mitigated by an appropriately chosen magnetic bias field. This enables Raman sideband cooling of a single atom close to its three-dimensional ground state (vibrational quantum numbers $\bar{n}_x = \bar{n}_y = 0.01, \bar{n}_z = 8$) even for a trap beam waist as small as $w = 900$ nm. The small atomic wavepacket with $\delta x = \delta y = 24$ nm and $\delta z = 270$ nm represents a promising starting point for future hybrid quantum systems where atoms are placed in close proximity to surfaces.

Single atoms in “optical tweezer” traps [1] are a promising resource for various applications in quantum science and engineering. They can be individually moved [2], manipulated [3, 4], read-out [5, 6], and used to implement quantum gates [7, 8], in a manner similar to trapped ions. At the same time, they may be strongly coupled to photonic [9, 10], plasmonic [11], or other solid-state systems [12–14], opening a new frontier for the realization of quantum networks and hybrid quantum systems. These intriguing applications require trapping single ultra-cold atoms near surfaces at distances well below an optical wavelength. While this is challenging for ions [15], and magnetically trapped atoms [12, 16], it is achievable with neutral atoms in optical dipole traps.

An optical tweezer can be efficiently loaded with a single atom from an optical molasses by making use of a light-induced two-body loss process (collisional blockade) [1, 17]. The temperature of an atom loaded in this way is in the range of $30 - 200 \mu\text{K}$ [3, 4, 7, 8, 10, 18, 19], at which point the atom has a characteristic root-mean-square (rms) spatial extent of $\delta r \approx 200$ nm and $\delta z \approx 1 \mu\text{m}$ in the radial and axial directions, respectively. This spatial spread is an impediment in several current experiments [7, 20], while the elevated temperature reduces the coherence time [3, 4, 7, 8, 19]. Moreover, interfacing the atom to the near field of a solid-state structure requires much stronger confinement, as in this case the atom must be localized on the scale of a reduced resonance wavelength $\lambda/2\pi = 120$ nm (for Rb).

These applications require significant improvements in laser cooling and coherent manipulation. Raman sideband cooling is a powerful technique to control atomic motion, as was demonstrated previously for ions and atomic ensembles in larger traps [21–25]. Coherent Raman transitions between two stable ground states that change the atom’s vibrational level can be used to remove energy, combined with an optical pumping process to remove entropy and complete the cooling cycle (Fig. 1a).

However, in very tightly confining traps with beam waist $w \sim \lambda$, polarization effects associated with the

breakdown of the paraxial approximation can strongly impede coherent manipulation and cooling. Such tightly focussed beams exhibit a longitudinal polarization component, which even for linearly polarized input fields results in spatially varying elliptic polarization [26–29]. The corresponding atomic-state-dependent trapping potentials reduce atomic coherence, induce force fluctuations, and impair cooling [30]. These effects are present not only in optical tweezers, but also at sub-wavelength distances from dielectric boundaries [10, 31], and in projected optical lattices to be used for many-body quantum simulation [32].

In this Letter, we present a detailed study of the longitudinal polarization component of a dipole trap formed by a high-numerical-aperture lens, demonstrate how the associated effect on a trapped atom can be partially compensated using a properly oriented magnetic bias field, and apply these results to perform Raman sideband cooling of a single atom. After cooling, the atom is in the ground state along the two radial directions ($\bar{n}_r = 0.01^{+0.06}_{-0.01}$), and occupies just a few quantum states ($\bar{n}_a = 8.1(8)$) in the axial trap direction. The corresponding rms size of the atomic wavepacket is given by the ground state length of $\delta r = 24$ nm in the radial directions, and a thermal extent $\delta z = 270$ nm in the axial direction. This represents a hundred-fold reduction in spatial volume, and a reduction by 10^4 in phase-space volume, over the starting conditions.

The longitudinal polarization component can be understood in the framework of ray optics (see Figure 1b). Light entering a lens consists of parallel rays with transverse linear polarization. Upon refraction the polarization of each ray must also deflect to remain transverse to the ray [26]. In the diffraction-limited volume around the focus, all rays interfere and the resulting field is elliptically polarized. Following Fig. 1b, two features emerge near the focus: the polarization vector is rotating in the plane set by the incident polarization vector and the optical axis, and the sense of this rotation is opposite above and below the optical axis.

For light that is far detuned compared to the excited-

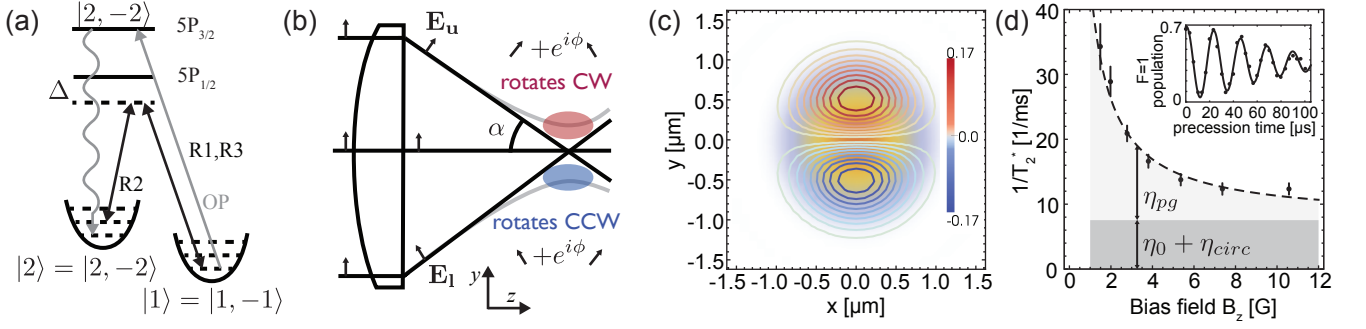


FIG. 1. (a) Relevant levels and transitions in ^{87}Rb . The eigenstates of the harmonic potential for the ground state are indicated with dashed lines. Atomic levels are defined in the $|F, m_F\rangle$ basis. See text for beam orientations and polarizations. (b) The origin of elliptical polarization near the focus (see text). (c) Cut through the focal plane for $\alpha = 0.43$. Contour lines show \tilde{C}_x , which is C_x scaled to the local intensity $|E(\vec{r})|^2/|E(\vec{r}_{max})|^2$. Background shading shows Gaussian intensity profile for comparison. (d) Dephasing rate between the states $|1\rangle$ and $|2\rangle$ as a function of bias field, with $\lambda_T = 815$ nm. The improvement at large bias fields is due to suppression of the polarization gradient. Fit is to model described in text: $\eta_0 + \eta_{circ}$ are background dephasing rates from the finite detuning and slight elliptical polarization of the dipole trap; η_{pg} arises from the longitudinal polarization. Inset: Ramsey measurement of dephasing rate between $|1\rangle$ and $|2\rangle$ at $B_z = 10.5$ G.

state hyperfine structure, the vector light shift for alkali atoms in the ground state is [33, 34]:

$$U(\mathbf{r}) = -U_0(\mathbf{r}) \frac{\delta_2 - \delta_1}{\delta_2 + 2\delta_1} \mathbf{C}(\mathbf{r}) \cdot g_F \hat{\mathbf{F}} \quad (1)$$

where $U_0(\mathbf{r})$ is the scalar dipole trap potential, δ_1 and δ_2 are the detunings from the D1 and D2 lines, respectively, $\epsilon(\mathbf{r})$ is the local (unit norm) polarization vector, $\hat{\mathbf{F}}$ is the total angular momentum operator and $g_F = [F(F+1) - I(I+1) + J(J+1)]/F(F+1)$. The vector $\mathbf{C} = \text{Im}[\epsilon(\mathbf{r}) \times \epsilon^*(\mathbf{r})]$ quantifies the direction and degree of ellipticity (with magnitude $|\mathbf{C}| = 1$ for circularly polarized light; 0 for linear polarization). Using the vector Debye integral [26], we have numerically computed the polarization near the dipole trap focus (Fig. 1c). The most important term is the polarization gradient dC_x/dy . For a lens with numerical aperture α , the maximum gradient, occurring at the beam focus, is well approximated by $3.1\alpha \sin \alpha/\lambda$ for uniform illumination of the lens aperture, and $2.6\alpha \sin \alpha/\lambda$ for illumination by a Gaussian beam with a $1/e^2$ diameter equal to the lens diameter. In the experiments presented here, $\alpha = 0.43$ and $\lambda = 815$ nm, so $dC_x/dy = 0.57/\mu\text{m}$. Since the state-dependent potential in Equation (1) is linear in $\hat{\mathbf{F}}$, it produces the same energy shifts as a magnetic field, so dC_x/dy can also be expressed as an effective magnetic-field gradient with magnitude $B'_x = 1.4$ G/ μm at the trap center (using $U_0 = 0.82$ mK).

In the absence of an externally applied magnetic bias field, trapping potentials corresponding to different magnetic sublevels m_F are displaced by $\Delta x = \mu_B \Delta(g_F m_F) B'_x / (m\omega_r^2)$, where $\mu_B \Delta(g_F m_F)$ is the difference in the magnetic moment. For $\Delta(g_F m_F) = 1/2$, the resulting displacement is $\Delta x = 11$ nm, which is non-negligible compared to the ground state length

$\sqrt{\hbar/2m\omega} = 24$ nm. While this state-dependent displacement could be useful for Raman cooling or other motional state manipulations [35, 36], it also leads to rapid internal-state decoherence on the timescale of the radial trap oscillation period.

This problem can be mitigated by applying a bias magnetic field $\mathbf{B} = B_z \hat{z}$ orthogonal to \hat{x} that suppresses the effective field gradient according to $B_{tot} = \sqrt{B_z^2 + (B'_x y)^2} \approx B_z + (B_x'^2/2B_z)y^2$. In this case, the gradient causes only a state-dependence in the strength of the harmonic trap potential. Superpositions of magnetic sublevels that experience different trapping potentials of the form $U_1(\mathbf{r}) = (1 + \eta)U_2(\mathbf{r})$ are dephased with a coherence time $T_2^* = 0.97 \times 2\hbar/(k_B T \eta)$ [30], where T is the temperature of the atom and k_B is the Boltzmann constant. In the presence of a large orthogonal bias field, the polarization gradient contributes to η as $\eta_{pg} = \mu_B \Delta(g_F m_F) B_x'^2 / (3m\omega^2 B_z)$ (the factor of 1/3 results from averaging over the three trap axes). We can use the dependence on B_z to accurately measure the polarization-induced gradient B' , and improve the atomic coherence by applying a large bias field B_z (Fig. 1d).

We measure the decoherence between the states $|1\rangle \equiv |F=1, m_F=-1\rangle$ and $|2\rangle \equiv |F=2, m_F=-2\rangle$ by loading a single atom into a tweezer trap with a depth of 1.6 mK at zero bias field, then ramping down the trap depth to 0.82 mK as we ramp up the bias field B_z to the desired value. The atom is optically pumped into $|2\rangle$, the hyperfine transition $|2\rangle \rightarrow |1\rangle$ is driven by a two-photon Raman process in a Doppler-free configuration, and the state detection is accomplished using a push-out beam, as described in more detail below. The coherence time T_2^* is extracted from a Ramsey-type measurement, using a fit to the function introduced in Ref. [30].

At two different trap wavelengths λ_T , we fit $1/T_2^* = 1.03(\eta_0 + \eta_{circ} + \eta_{pg})(k_B T/2\hbar)$. The only free parameters are the degree of circular polarization in the incident dipole trap beam due to uncompensated birefringence along the beam path (η_{circ}) and the strength of the effective field gradient B'_x . The temperature is determined independently ($T = 40\mu\text{K}$ for this measurement, see below for technique). η_0 reflects the different trapping potentials for $F = 1$ and $F = 2$ atoms due to the finite trap detuning. At $\lambda_T = (802, 815)\text{ nm}$, we find $B'_x = (2.4, 1.4)\text{ G}/\mu\text{m}$, and thus $dC_x/dy = (0.46(6), 0.54(3))/\mu\text{m}$, in reasonable agreement with our estimate of $0.57/\mu\text{m}$.

Having developed a detailed understanding of trap-induced decoherence in this system, we now turn to Raman sideband cooling. We use three orthogonal running-wave fields to drive Raman transitions, labeled R1-R3 (Fig. 1a). R1 propagates anti-parallel to the dipole trap ($-\hat{z}$) and is circularly polarized to drive σ_- transitions. R2 propagates along \hat{x} and is circularly polarized; R3 propagates along \hat{y} and is linearly polarized along \hat{x} . Optical pumping to the $|2\rangle$ state is provided by circularly polarized beams co-propagating with R1, addressing the $F = 1 \rightarrow F' = 2$ and $F = 2 \rightarrow F' = 2$ transitions on the D2 line. The frequencies of the lasers are set to the measured resonances in the dipole trap, which are shifted by $\sim 30\text{ MHz}$ from the resonances in free space; the intensities are about 100 times less than saturation. We measure the $F = 1$ population by pushing out any atom in $F = 2$ using a circularly polarized beam along the optical pumping path that is resonant with the $F = 2 \rightarrow F' = 3$ transition on the D2 line, then measuring whether the atom has remained trapped by turning the molasses back on.

In a typical experiment, we load an atom from the MOT into the optical dipole trap with a depth of 1.6 mK at zero bias field, then decrease the trap depth to 0.82 mK while ramping the bias field B_z up to 7.5 G . Lowering the trap depth serves to increase the coherence time while leaving the trap frequencies high enough that sideband cooling is still achievable, with $(\omega_r, \omega_a) = 2\pi \times (100, 15.6)\text{ kHz}$. All temperatures reported in this paper are measured in the 0.82 mK deep trap. We cool the atoms in the following sequence: we first apply the R2 and R3 beams (Fig. 1) and the optical pumping beams together for 10 ms to continuously cool the radial modes; then, we perform ten cycles consisting of 2 ms of axial cooling using the R1 and R2 beams, followed by 4 ms of radial cooling using the R2 and R3 beams again. This sequence prevents the radial modes from heating while the axial cooling proceeds.

The parameters for the first radial cooling phase are optimized by measuring the temperature using a release and recapture technique [37]. This data, shown in Figure 2a, is fit using a Monte-Carlo simulation [18]. The initial kinetic energy per dimension K is such that

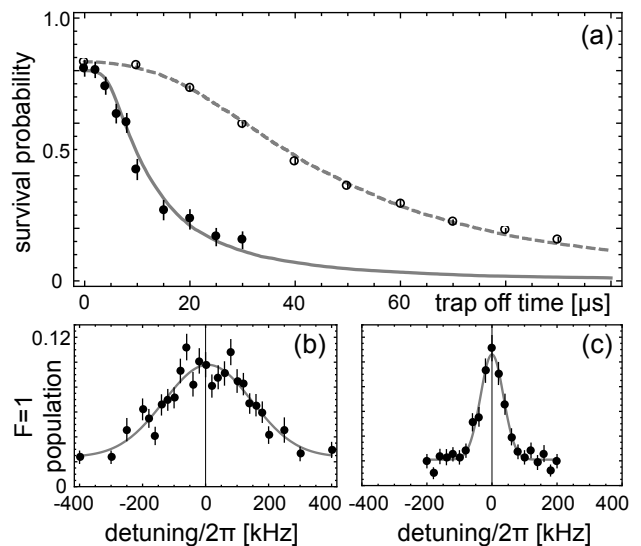


FIG. 2. (a) Release and recapture temperature measurement. (Closed, open) circles show measurements (before, after) radial cooling. A Monte Carlo model yields kinetic energies K such that $2K/k_B = 52(4)\mu\text{K}$ before cooling, and $(2K_r/k_B, 2K_a/k_B) = (2.4(1), 158(14))\mu\text{K}$ after cooling. (b,c) Doppler measurement of the axial kinetic energy before and after cooling the axial mode. (b) After radial cooling only, $2K_a/k_B = 129(19)\mu\text{K}$. (c) After radial and axial cooling, $2K_a/k_B = 8.1(1)\mu\text{K}$.

$2K/k_B = 52\mu\text{K}$. The measurement after cooling yields anisotropic kinetic energies of $2K_r/k_B = 2.4(1)\mu\text{K}$ in the radial direction and $2K_a/k_B = 158(14)\mu\text{K}$ in the axial direction (the release and recapture technique is only weakly sensitive to the axial mode). The fitted kinetic energies represent the global minimum in χ^2 over the entire space of three independent energies for each axis, including unphysical temperatures less than the ground state energy $\hbar\omega/2k_B = 2.4\mu\text{K}$ for the radial modes. The agreement of the measured kinetic energy with that of the zero-point motion suggests that we have reached the radial ground state after this cooling phase alone. The radial cooling works best with a two-photon Rabi frequency $\Omega_{R2,R3} = 2\pi \times 17\text{ kHz}$ and a detuning of $-\omega_r = -2\pi \times 100\text{ kHz}$ from the two-photon resonance.

To characterize the axial temperature independently after the radial cooling, we measure the Doppler width of the $|2\rangle$ to $|1\rangle$ transition when driven with the R1 and R2 beams. The wavevector $\Delta\mathbf{k}_{12} = \mathbf{k}_{R1} - \mathbf{k}_{R2}$ has a projection onto the axial and radial directions, but the Doppler profile should mostly be sensitive to the axial mode here since the radial degrees of freedom are already cold. After the first stage of radial cooling, we measure a kinetic energy of $2K_a/k_B = 129(19)\mu\text{K}$ (Fig. 2b). After optimization, we obtain a feature with a width corresponding to $2K_a/k_B = 8.1(1)\mu\text{K}$ (Fig. 2c). This data

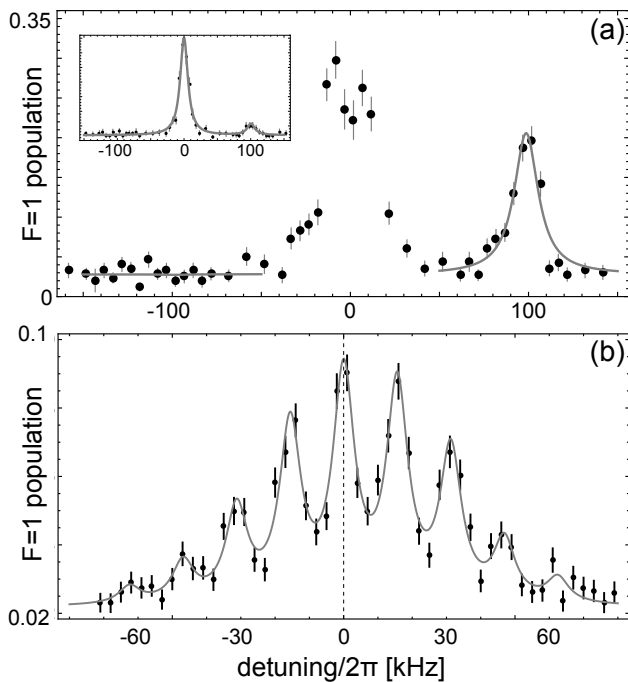


FIG. 3. Sidebands showing final occupations in the (a) radial and (b) axial directions. In (a), the red and blue sideband amplitudes are fit to independent lorentzians; their ratio yields a radial temperature $\bar{n}_r = 0.01^{+0.06}_{-0.01}$. Inset: same measurement with shorter pulse length so the carrier is also resolved. In (b) 9 peaks are fit with independent heights, but equal spacings and widths. The heights are well-described by a thermal distribution with $\bar{n}_a = 8.1(1)$.

is fitted to a Gaussian, which conservatively assumes no power broadening. The optimum cooling parameters are a two-photon Rabi frequency of $\Omega_{R1,R2} \sim 2\pi \times 5$ kHz and a detuning of $-2\pi \times 60$ kHz. The parameters used for the interleaved radial cooling phases are the same as above.

To obtain more precise measurements of the final temperature of the atom, we resolve the asymmetric motional sidebands along two axes. The ratio of the sideband amplitude gives information about the vibrational state occupation of the atom [21]. Figure 3a shows the sidebands measured in the radial direction with small $\Omega_{R2,R3}$. The blue sideband is essentially absent, with a fitted amplitude 100 times smaller than the red sideband. From this, we extract a radial mode occupation of $\bar{n}_r = 0.01^{+0.06}_{-0.01}$. We do not know to what extent the two radial modes are non-degenerate or what the natural axes are, but from the release-and-recapture data showing that both modes must be very cold, and the fact that the spectrum shown here does not change if we measure it at a different time after the cooling (up to 100 ms later), we infer that the two modes are not perfectly degenerate and the R2+R3 beams address both modes. Therefore, we con-

clude that this spectrum reflects the temperature of both radial modes.

We also resolve the axial motional sidebands using the R1 and R2 beams at very low power, and observe a spectrum with nine peaks that is slightly asymmetric (Fig. 3b). We find that the ratios of the measured peak heights correspond very well to a thermal distribution $\rho_{nn} \propto \exp(-n/\bar{n}_a)$ with a mean vibrational number $\bar{n}_a = 8.1(8)$. The corresponding energy $(\bar{n}_a + 1/2)\hbar\omega_a = 6.5 \mu\text{K} \times k_B$ is similar to the result of the Doppler measurement above.

Several properties of the cooled atom are worth noting. The heating rate for the radial degrees of freedom is very low, less than $\Delta\bar{n} < 0.3$ over 200 ms. We observe no heating while translating the atom over distances $\sim 20\mu\text{m}$ in ~ 10 ms using a scanning galvanometer mirror. Decreasing the Rabi frequency $\Omega_{R1,R2}$ and detuning during the last cooling phase does not decrease the final axial temperature. This is possibly due to the fact that we cannot separately address the axial mode, or to our choice to optically pump along the axial direction, resulting in more heating along that direction. We are not aware of any fundamental effects that would prevent cooling to the ground state in this system.

It may be possible to extend the demonstrated method to perform high-fidelity state detection [5, 6] while cooling within one hyperfine state, and collecting optical pumping photons. Furthermore, it should also be possible to cool small ensembles of atoms held in arrays of traps [17] or together in a single trap. In the latter case, Raman cooling is advantageous compared to an optical molasses, in that the detuning of the optical pumping beam can be chosen over a wide range, allowing the effects of light assisted collisions [38] and heating due to rescattered photons [24] to be reduced.

We acknowledge funding from the NSF, CUA, DARPA, AFOSR MURI, the Packard Foundation and EU project AQUAT. JDT acknowledges support from the Fannie and John Hertz Foundation and the NSF GRFP.

Note After completion of this work, we have become aware of a related demonstration of Raman sideband cooling in an optical tweezer [39].

-
- [1] N. Schlosser, G. Reymond, I. Protsenko, and P. Grangier, *Nature* **411**, 1024 (2001).
 - [2] J. Beugnon, C. Tuchendler, H. Marion, A. Gaëtan, Y. Miroshnychenko, Y. R. P. Sortais, A. M. Lance, M. P. A. Jones, G. Messin, A. Browaeys, et al., *Nature Physics* **3**, 696 (2007).
 - [3] D. D. Yavuz, P. B. Kulatunga, E. Urban, T. A. Johnson, N. Proite, T. Henage, T. G. Walker, and M. Saffman, *Physical Review Letters* **96**, 063001 (2006).
 - [4] M. P. A. Jones, J. Beugnon, A. Gaëtan, J. Zhang, G. Messin, A. Browaeys, and P. Grangier, *Physical Re-*

- view A **75**, 4 (2007).
- [5] M. Gibbons, C. Hamley, C.-Y. Shih, and M. Chapman, *Physical Review Letters* **106**, 133002 (2011).
 - [6] A. Fuhrmanek, R. Bourgain, Y. Sortais, and A. Browaeys, *Physical Review Letters* **106**, 133003 (2011).
 - [7] E. Urban, T. Johnson, T. Henage, L. Isenhower, D. D. Yavuz, T. G. Walker, and M. Saffman, *Nature Physics* **5**, 110 (2009).
 - [8] A. Gaëtan, Y. Miroshnychenko, T. Wilk, A. Chotia, M. Viteau, D. Comparat, P. Pillet, A. Browaeys, and P. Grangier, *Nature Physics* **5**, 115 (2009).
 - [9] D. Alton, N. Stern, T. Aoki, H. Lee, E. Ostby, K. Vahala, and H. Kimble, *Nature Physics* **7**, 159 (2011).
 - [10] E. Vetsch, D. Reitz, G. Sagué, R. Schmidt, S. T. Dawkins, and A. Rauschenbeutel, *Physical Review Letters* **104**, 203603 (2010).
 - [11] D. E. Chang, J. D. Thompson, H. Park, V. Vuletic, and M. D. Lukin, *Physical Review Letters* **103**, 123004 (2009).
 - [12] D. Hunger, S. Camerer, T. W. Haensch, D. Koenig, J. P. Kotthaus, J. Reichel, and P. Treutlein, *Physical Review Letters* **104**, 143002 (2010).
 - [13] M. Hafezi, Z. Kim, S. L. Rolston, L. A. Orozco, B. L. Lev, and J. M. Taylor, *Physical Review A* **85**, 020302 (2012).
 - [14] P. Rabl, D. DeMille, J. Doyle, M. Lukin, R. Schoelkopf, and P. Zoller, *Physical Review Letters* **97**, 33003 (2006).
 - [15] N. Daniilidis, S. Narayanan, S. A. Moeller, R. Clark, T. E. Lee, P. J. Leek, A. Wallraff, S. Schulz, F. Schmidt-Kaler, and H. Haefner, *New Journal Of Physics* **13**, 013032 (2011).
 - [16] Y. Lin, I. Teper, C. Chin, and V. Vuletić, *Physical Review Letters* **92**, 50404 (2004).
 - [17] T. Grönzweig, A. Hilliard, M. McGovern, and M. F. Andersen, *Nature Physics* **6**, 951 (2010).
 - [18] C. Tuchendler, A. M. Lance, A. Browaeys, Y. R. P. Sortais, and P. Grangier, *Physical Review A* **78**, 9 (2008).
 - [19] W. Rosenfeld, F. Hocke, F. Henkel, M. Krug, J. Volz, M. Weber, and H. Weinfurter, *Physical Review Letters* **101**, 260403 (2008).
 - [20] M. K. Tey, G. Maslennikov, T. CH Liew, S. A. Aljunid, F. Huber, B. Chng, Z. Chen, V. Scarani, and C. Kurtz, *New Journal Of Physics* **11**, 043011 (2009).
 - [21] C. Monroe, D. Meekhof, B. King, S. Jefferts, W. Itano, D. Wineland, and P. Gould, *Physical Review Letters* **75**, 4011 (1995).
 - [22] S. Hamann, D. Haycock, G. Klose, P. Pax, I. Deutsch, and P. Jessen, *Physical Review Letters* **80**, 4149 (1998).
 - [23] H. Perrin, A. Kuhn, I. Bouchoule, and C. Salomon, *EPL (Europhysics Letters)* **42**, 395 (1998).
 - [24] A. Kerman, V. Vuletic, C. Chin, and S. Chu, *Physical Review Letters* **84**, 439 (2000).
 - [25] D. Han, S. Wolf, S. Oliver, C. McCormick, M. DePue, and D. Weiss, *Physical Review Letters* **85**, 724 (2000).
 - [26] B. Richards and E. Wolf, *Proceedings of the Royal Society A: Mathematical, Physical and Engineering Sciences* **253**, 358 (1959).
 - [27] A. Rohrbach, *Physical Review Letters* **95**, 168102 (2005).
 - [28] O. M. Maragò, P. H. Jones, F. Bonaccorso, V. Scardaci, P. G. Gucciardi, A. G. Rozhin, and A. C. Ferrari, *Nano Letters* **8**, 3211 (2008).
 - [29] P. J. Reece, W. J. Toe, F. Wang, S. Paiman, Q. Gao, H. H. Tan, and C. Jagadish, *Nano Letters* **11**, 2375 (2011).
 - [30] S. Kuhr, W. Alt, D. Schrader, and I. Dotsenko, *Physical Review A* p. 023406 (2005).
 - [31] C. Lacroûte, K. Choi, A. Goban, D. Alton, D. Ding, N. Stern, and H. Kimble, *New Journal Of Physics* **14**, 023056 (2012).
 - [32] W. S. Bakr, J. I. Gillen, A. Peng, S. Fölling, and M. Greiner, *Nature* **462**, 74 (2009).
 - [33] I. H. Deutsch and P. S. Jessen, *Physical Review A* **57**, 1972 (1998).
 - [34] K. Corwin, S. Kuppens, D. Cho, and C. Wieman, *Physical Review Letters* **83**, 1311 (1999).
 - [35] L. Förster, M. Karski, J. Choi, A. Steffen, W. Alt, D. Meschede, A. Wiedera, E. Montano, J. Lee, W. Rakreungdet, et al., *Physical Review Letters* **103**, 233001 (2009).
 - [36] X. Li, T. Corcovilos, Y. Wang, and D. Weiss, *Physical Review Letters* **108**, 103001 (2012).
 - [37] P. Lett, R. Watts, C. Westbrook, W. Phillips, P. Gould, and H. Metcalf, *Physical Review Letters* **61**, 169 (1988).
 - [38] M. McGovern, A. J. Hilliard, T. Grönzweig, and M. F. Andersen, *Optics Letters* **36**, 1041 (2011).
 - [39] A. M. Kaufman, B. J. Lester, and C. A. Regal, *arXiv physics/atom-ph* p. 1209.2087v1 (2012).